Alessandro PIRONDI* and Claudio DALLE DONNE**

Mixed Mode Fracture of a Ferritic Steel: J-Integral against CTOD.

* Department of Industrial Engineering - University of Parma, Viale delle Scienze, I-43100 Parma, Italy
** German Aerospace Research Establishment, Institute of Materials Research, Linder Höhe, D-51147 Köln, Germany

Keywords: ductile fracture, mixed mode fracture, crack resistance curve, crack tip opening displacement, J-integral.

ABSTRACT: Mixed mode I/II stable crack growth experiments in a ferritic steel were carried out using CTS (Compact Tension Shear) specimens. It is shown that predominant mode II loading drove the crack in the direction almost parallel to the fatigue pre-crack, whereas high mode I crack tip opening caused a crack path deviation. The mixed-mode crack resistance curve is presented in form of the crack tip displacement vector $\delta_v=(\delta_I^2+\delta_{II}^2)^{0.5}$ *and in form of the J-integral, which was calculated from the load-displacement curves using specifically developed plastic* η*-factors. The suitability of the two parameters to describe mixed-mode ductile fracture is discussed and it is shown that* δ_v *is more appropriate.*

Introduction

The work concerning mixed-mode I/II fracture has been predominantly restricted to linear elastic fracture mechanics (LEFM) and thus to brittle materials. In many practical situations where ductile engineering material are involved, the loading experienced at a crack tip can be very complex, resulting in ductile mixed mode fracture. In these cases the failure behaviour cannot be predicted with LEFM models.

Only recently some experimental investigations (1-3) and FE simulations (4-6) have been devoted to the study of mixed-mode I/II ductile fracture. It has been generally found that a non uniform damage field surrounds an initially smooth notch tip under mixed mode loading, **Fig. 1**. One side of the notch, dominated by tensile stresses, blunts while the opposite side sharpens as a consequence of predominant shear strains. Two distinguished and competing fracture mechanisms are therefore present at the notch tip: a mode I, tensile fracture mechanism at the blunted part and a mode II, shear mechanism at the sharpened part of the deformed notch. The prevalence of one of the two fracture mechanisms depends on loading mixity, work hardening behaviour and microstructure (presence and extent of porosities, inclusions,...). In case of mode I tensile crack growth from the blunted side of the notch or crack, it is well known, that the main damaging mechanism in ductile materials is void growth and coalescence. However in homogeneous, low work-hardening materials, like ferritic steels

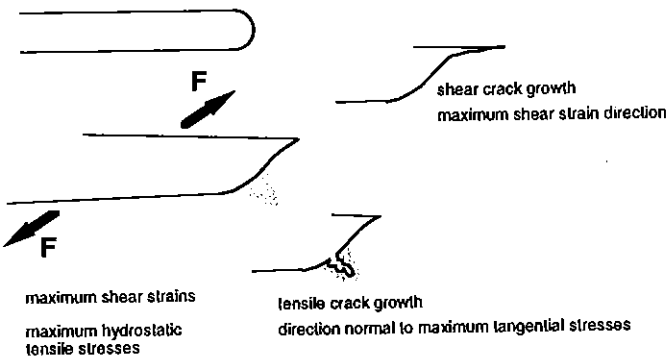

Fig. 1 Effect of mixed mode loading on crack tip deformation and crack propagation in ductile materials.

in the upper shelf, a small amount of mode II loading likely causes the formation of an intense shear band at the sharpened part of the crack tip along which the crack propagates (mode II fracture type) (2, 3, 7-9). Reasons for this behaviour could be porosities and inclusions too small and isolated to grow and coalesce under tension (mode I fracture type) together with the loss of crack tip constraint (and therefore shear localisation) under mode II loading (6).

Values of mixed-mode fracture toughness are clearly dependent on the actual crack propagation mode and the used fracture parameter. Low work hardening, ductile materials often display a decrease of J-initiation values and tearing resistance curves with increasing mode II components (2, 8, 10), whereas materials which fracture under small scale yielding generally show higher mode II crack resistance values (11, 12). These trends are however linked to the J-integral definition of fracture toughness and therefore on the influence of the degree of specimen plastification on the critical J-values (see below).

The aim of this paper is to experimentally investigate plane stress mixed-mode crack growth in a ferritic steel using thin CTS specimens. Attention was focused on the crack path and on the mixed-mode crack resistance curve, in attempt to verify the suitability of the crack tip displacement vector δ_v and/or the J-integral to describe mixed-mode fracture.

Experimental Procedure

Fracture tests at 15°, 45°, 75° and 90° loading angles were carried out with 4-mm thick CTS specimens (13) mounted on the testing rig shown in **Fig. 2**. The material tested was a fine grained structural steel with the german designation „StE 550" (yield strength plateau at 580 MPa and ultimate strength 650 MPa).

Most of the mirror-polished CTS specimens were pre-cracked in mode I up to $a_0/W = 0.6$. To achieve significant stable crack extensions in the near mode II (loading angle $\phi \geq 75°$) loaded specimens, longer pre-crack length to width ratio ($a_0/W = 0.67$) were necessary. In all cases the fatigue crack length was monitored by the DC potential drop method.

Before the actual mixed mode experiment the specimens were removed from the servohydraulic testing machine and a grid with 0.5 mm pitch was traced around the fatigue crack tip with a microhardness testing device, **Fig. 3**. Thereafter the CTS-set-up was installed in the desired loading direction and instrumented with the anti-buckling plates and two cross-mounted clip gages. These clip gages allowed the measurement of the mode I crack opening displacement cod_I and mode II crack sliding displacement cod_{II} at 17mm from the specimen border, **Fig. 4**. The quasistatic stable crack growth experiments were then performed under displacement controlled conditions. A series of photographs of the blunting and propagating crack was taken through the microscope during each test. The values for the opening displacement δ_I and for the sliding displacement δ_{II} could be evaluated directly from these photographs. This was done by measuring the relative displacement of the intersection points of the fatigue crack flanks with the vertical reference line (0.5 millimetre behind the fatigue crack tip, **Fig. 3**).

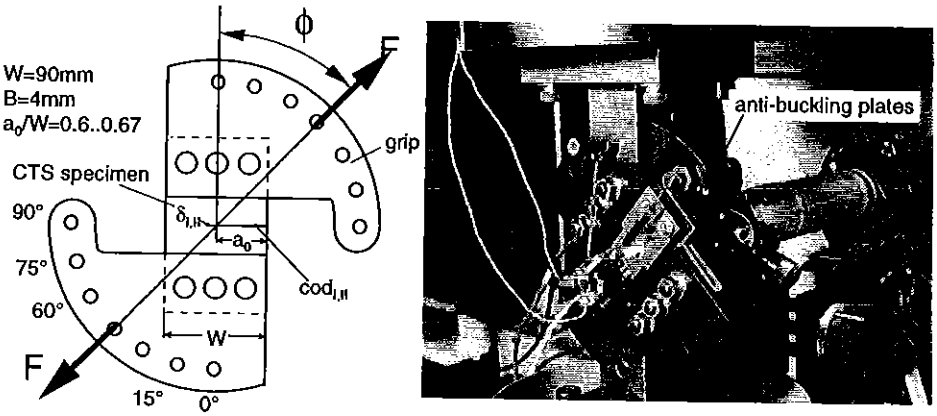

Fig. 2 CTS specimen, loading device and instrumentation. Note the anti-buckling plates on the right picture.

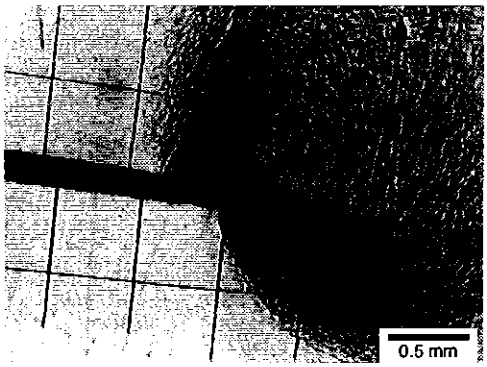

Fig. 3 Crack tip of a 45°-loaded specimen. The crack tip opening (δ_I) and sliding (δ_{II}) displacements were taken by measuring the relative displacement of the intersection points of the fatigue crack flanks with the first vertical reference line behind the fatigue crack tip.

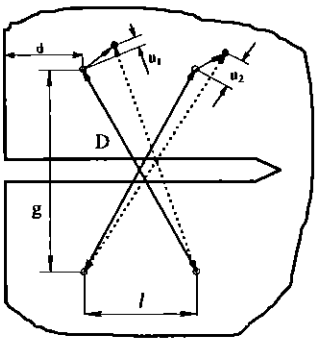

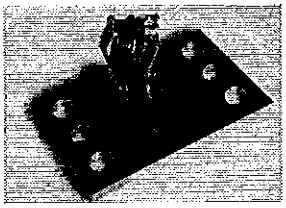

$$cod_{II} = \frac{1}{4l}(u_1 + u_2)|u_1 - u_2|$$

$$cod_I = \sqrt{(u_1 + D)^2 - (cod_{II} + l)^2} - g$$

$$cod_v = \sqrt{cod_I^2 + cod_{II}^2}$$

g = 15mm l = 10mm d = 12mm

Fig. 4 Measurement of cod_I and cod_{II} at 17 mm from the specimen border (14).

After unloading specimens were cycled again under mode I fatigue, to mark the final shape of the stable crack front. The amount of stable crack propagation was then measured optically and the average of both specimen halves was taken as the Δa-value for the multiple-specimen presentation of the results. This is an important aspect, since near mode II loaded specimens showed different amounts of stable shear crack growth on the mating crack surfaces (15, 16). A step-by-step displacement-refocusing procedure through a microscope with a micrometric focusing system was used to record the crack surface profile in growth direction. A mean crack propagation angle α was calculated from such data. In this paper only the angles measured on the extended side of the two mating crack surfaces of each specimen are presented.

Fracture Parameters

According to FE calculations (6, 17) and the experimental experiences (8, 17, 18) the magnitude of the crack tip displacement vector δ_v , expressed as a function of δ_I (opening) and δ_{II} (sliding) components

$$\delta_v = \sqrt{\delta_I^2 + \delta_{II}^2} \tag{1}$$

is considered as a candidate parameter for an unambiguous characterisation of material failure. In the quoted references it was shown, that similar definitions of crack or notch tip deformation lengths had nearly constant values at incipient crack growth for various levels of mode mixity, whereas the J-integral value at initiation decreased with increasing mode II components.

Following the work presented in (15) the δ_v-values were taken from the scribed lines behind the fatigue pre-cracks even in the case of growing cracks, **Fig. 3**. This simple measurement technique allowed a comparison of the mixed mode crack resistance curves with mode I δ_5-R-curves of C(T)- and M(T)-specimens (16). The δ_5 clip gage measures the relative displacement of two points located in a distance of 2.5 mm on either side of the fatigue pre-crack tip in mode I (19). Recently Amstutz et al. presented displacement values at a tip of a growing mixed mode crack (20).

The J-integral was chosen as a second candidate parameter to display the crack resistance curves. Like in mode I it is generally evaluated from the area under the load-displacement curve also in the mixed-mode or mode II loading cases (2, 11, 21-23). According to the usual procedure (24) J is divided into an elastic part J_{el} and a plastic part J_{pl}. These two components can be written as (plane stress):

$$J_{el} = \frac{K_I^2 + K_{II}^2}{E} \tag{2}$$

$$J_{pl} = \eta_{pl} \frac{U_{pl}}{B(W-a)} \tag{3}$$

where U_{pl} is the plastic work done by the applied load and η_{pl} is the plastic η-factor. The elastic component can be readily determined from the stress intensity factor solutions of (13) as a function of the applied load. Like in the work of Jeon (23) (asymmetric four point bending specimen), the plastic part of J is estimated under the assumption that the mode I η_{pl}-derivation of Bucci et al. (25) is applicable also for cracks under mixed mode loading. For ideal plasticity and constant load line displacement J_{pl} can be written as:

$$J_{pl} = -\frac{1}{B}\frac{\partial U_{pl}}{\partial a} = -\frac{1}{F_{pl}}\frac{\partial F_{pl}}{B\partial a}U_{pl} \tag{4}$$

where F_{pl} is the plastic limit load. Combining (3) and (4) yields:

$$\eta_{pl} = -\frac{W-a}{F_{pl}}\frac{\partial F_{pl}}{\partial a} \tag{5}$$

With the mixed mode limit load for superimposed tension, bending and shear from (26) (Chapter 2.13.4) following expression for the η_{pl} factor is obtained:

$$\eta_{pl} = 1 + \frac{0.75\cos\phi\dfrac{W}{b}\left(1+\dfrac{f_1}{f_2}\right)}{\dfrac{4\sin^2\phi}{(f_1+f_2)} + f_1 + f_2} \tag{6}$$

where

$$b = (W-a)$$

$$f_1 = 0.75\cos\phi\frac{a}{b} \tag{6 bis}$$

$$f_2 = \sqrt{\left(0.75\cos\phi\frac{a}{b}\right)^2 + \cos^2\phi}$$

For a/W=0.5 the developed η_{pl}-function agrees with the finite element analysis (FEA) of a single edge notched specimen (SEN) under mixed mode loading in a very stiff fixture (2). This is shown in **Fig. 5**, where the η_{pl}-factors are plotted as a function of the applied mixed mode ratio expressed through M_e (defined in **Fig. 5**). Mode I and mode II η_{pl}-values of a pin-loaded SEN-specimen (27) and a compact tension shear specimen (22), both similar to the investigated CTS configuration, are also included in the diagram.

The J-analysis required a U_{pl}-evaluation from the plastic load line displacement versus force curve. In the CTS specimens the load line corresponds to the specimen centreline and it was therefore necessary to interpolate the load line $cod_{I,LL}$ linearly from the clip gage readings and the δ_I-values measured at the fatigue crack tip. The corrected $cod_{I,LL}$ and the cod_{II} values were then projected on the load line to give the load line displacement cod_{LL}. The plastic component U_{pl} was obtained by subtracting the elastic work from the total work. Since the investigated crack propagations were

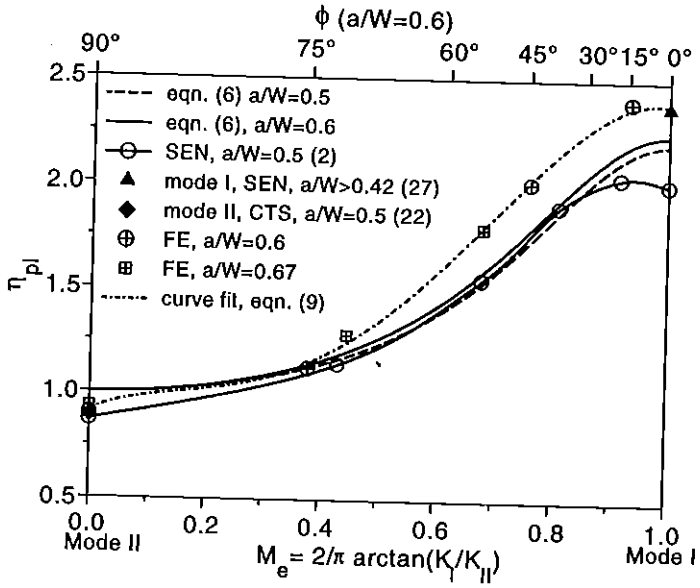

Fig. 5 Dimensionless η_{pl}-factors for SEN and CTS specimens under mode I, mode II and mixed mode loading conditions.

relatively small, the initial linear cod_{LL}-F relationship was used to calculate the stored elastic energy at the end of the tests.

Another technique for the experimental evaluation of the mixed mode J-Integral was presented by Thogo and Ishii (11). They calculated $J_{pl,I+II}$ for asymmetric three and four point bending from the sum of mode I and mode II contributions:

$$J_{pl,I+II} = \frac{1}{B(W-a)}\left(\eta_{pl,I} U_{pl,I} + \eta_{pl,II} U_{pl,II}\right) \tag{7}$$

where $\eta_{pl,I}$ and $\eta_{pl,II}$ corresponded to pure mode I and pure mode II loading respectively. Consequently $U_{pl,I}$ ($U_{pl,II}$) was calculated from the mode I (mode II) components of plastic displacement and force. Here the method of Thogo and Ishii led to

$$J_{pl,I+II} = \frac{1}{B(W-a)}\left(2.38\, U_{pl,I} + 0.9\, U_{pl,II}\right) \tag{8}$$

with $\eta_{pl,I}$ taken from the pin loaded SEN specimen (27) and $\eta_{pl,II}$ taken as an average of the known literature values (2, 22) of CTS-like specimens under pure mode II loading. The elastic J-component

still equalled equation (4). Finally, it is important to note, that the developed J-estimations are only valid for small and coplanar crack propagations.

Finite Element Calculations

To check the validity of the J-estimation formulas of the previous section two-dimensional, plane stress finite element (FE) analyses of CTS specimens were performed using conventional small strain theory, incremental plasticity with associated v. Mises flow rule and isotropic hardening. The analyses were conducted using the ABAQUS code on an HP 712/80 workstation. The investigated CTS specimens had crack-to-width ratios of a/W=0.6 and 0.67. Loading angles of ϕ=15°, 45°, 75° and 90° and ϕ=60°, 75° and 90° were considered respectively. Crack growth was not examined.

In **Fig. 6** the FE model of a CTS specimen loaded at ϕ=75° is represented. The mesh was build up with isoparametric, eight-noded elements. A circular core with quarter-point collapsed elements surrounded the crack tip. This modelling produced the 1/r-singularity appropriate for plastic crack tip fields. The high stiffness fixtures were simulated by the rigid beam frames visible in **Fig. 6**. The position of load introduction could be varied to generate different mixed-mode ratios. The lower frame extremity was pinned at a fixed location while the load was applied to the upper frame. During the loading procedure the load point displacement direction was constrained into the defined loading direction. The connection between the specimen and the frame was simulated with rigid cylindrical surfaces (whose contact points with the specimen are represented by the triangles in **Fig. 6**). A "softened" contact pressure-clearance law was defined to avoid convergence problems when solving the contact conditions. Under elastic loading conditions the difference between the obtained J_{el} values and the ones presented in (13) were always smaller than 10%. This difference was mainly due to the different load application used in (13). For the elastic-plastic calculations the true stress and strain data of StE 550 steel was used as material model. The J-values on several paths around the crack tip were directly taken from the ABAQUS output. As shown in (28), the region with path dependent J-values around the crack tip increased with increasing mode II loading components.

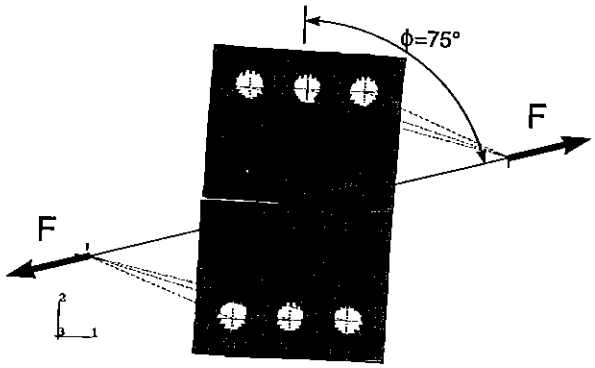

Fig. 6 Finite element model of the CTS specimen with a/W=0.6 under a loading angle of 75° (deformed mesh).

In **Fig. 7** the numerically obtained J-values are plotted as a function of the load line displacement for the CTS-specimens with a/W=0.6 under different loading angles. These curves are compared to the J-values calculated from the areas under the load displacement curves, just like the experiments, following the formulas (6) and (8) for J_{pl} and formula (2) for J_{el}. Both methods agree quite well with the finite element records. In the case of 75°-loading the differences between the estimated and the finite element J are attributed to J_{el}, as stated previously. Especially for the near mode I loaded specimens ($\phi \leq 45°$) the method of Thogo and Ishii (eqn. (8)) yields more accurate results, because the analytically developed η_{pl}-formula (6) apparently underestimates the real η_{pl} in mode I. This is also shown in **Fig. 5**, where the η_{pl}-values extracted from the FE calculations are compared to the analytical results (crossed symbols in **Fig. 5**). Interestingly in the small range of investigated crack lengths the a/W-effect on η_{pl} is covered by the change in mixed mode ratio M_e. This suggests following fit of the FE results:

$$\eta_{pl,FE} = 0.915 + 1.141 M_e - 5.566 M_e^2 + 14.1 M_e^3 - 8.191 M_e^4 \qquad (9)$$

which should be valid for $0.6 \leq a/W \leq 0.7$. The experimentally evaluated J (eqns. (2), (3) and (9)) is referred to as J_{FE}. In the next section the J_{FE}-Δa crack resistance curves are compared to the J_{I+II}-R-curves assessed with the method of Thogo and Ishii.

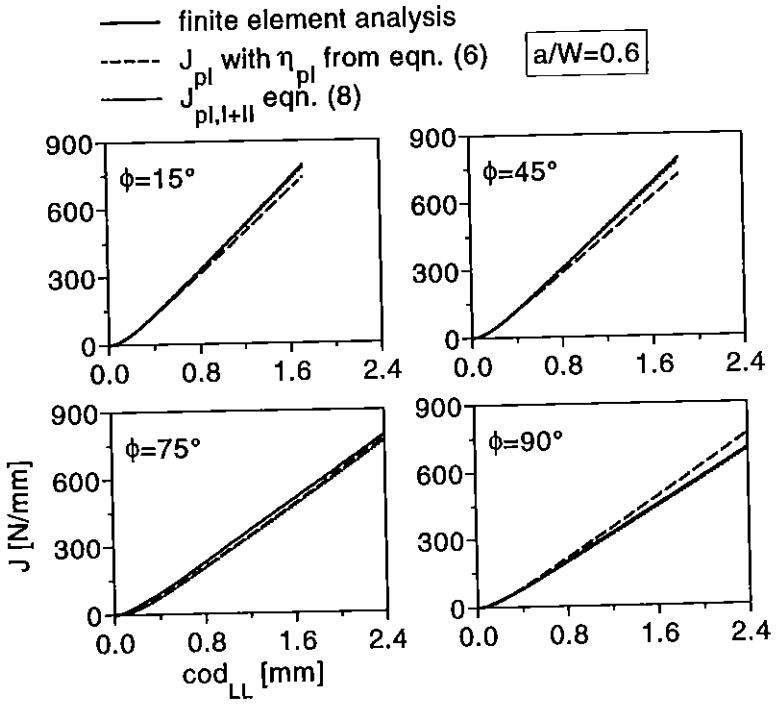

Fig. 7 J-values obtained directly from the finite element code compared to the J-values calculated from the areas under the load versus load line displacement (cod_{LL}) curves.

Results and Discussion

Two types of crack growth were observed in the ductile steel specimens, which fractured under ligament yielding conditions. Near mode I tested specimens ($M_e \geq 0.68$) failed in a manner similar to the one observed in mode I (referred to as „tensile crack growth"). The crack first diverted normally to the loading axis and changed then into a fracture path slanted at 45° to the thickness direction (15). Predominant mode II loading drove the crack ($M_e < 0.68$) in a direction almost parallel to the fatigue pre-crack. This „shear crack growth" is often observed in ferritic steels under mixed mode loading (1-3, 7, 8, 30). Further insights on the microscopic fracture appearance are given in (15, 16, 31). The stable crack deflection results are summarised in **Fig. 8**. The symbols denote the crack deflection angles α measured on the longer crack side of the CTS specimens and cruciform specimens with slanted cracks investigated in another paper (15). The predicted directions of maximum tangential stresses and maximum shear according to a small-scale yielding (SSY), plane strain analysis (29) for a Ramberg-Osgood material with the work hardening exponent N=15 are drawn with solid lines in **Fig. 8**. In (15) it was shown, that there is no considerable difference between the SSY plane strain

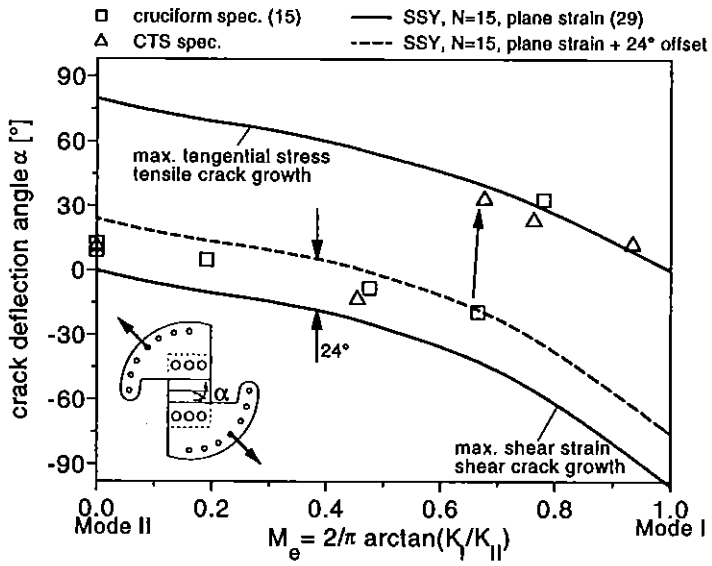

Fig. 8 Experimental crack deflection angles of CTS and cruciform specimens (15) versus applied mixed mode ratio compared to plane strain predictions (29).

and plane stress estimations. It appears that near mode I loaded, kinked tensile cracks followed a maximum tangential stress criterion. Moderate mode II components induced shear controlled failure. The transition from the tensile fracture to the shear fracture occurred at a mixed mode ratio (M_c=0.67) which was found also in other investigations with ferritic steels (1, 2, 8, 32).

The constant offset between the predicted and the measured shear deflection angles together with the dimples on the shear crack surfaces detected in (15, 31), suggested that the so called „shear crack" was in fact a combination of sliding off and void coalesce (33). The opened shear cracks did not progress exactly along a shear band, but at an certain offset angle giving a higher stress triaxiality (6). Probably the crack deviated from the negative hydrostatic stress states in the shear band region (6), to allow a microvoid sheeting mechanism to take part. This type of failure was successfully modelled by Kardomateas et al. (34). Their prediction of a (mode mixity independent) offset angle of 24° to the maximum shear strain direction for an N=13 material was very close to the results of the steel StE 550 specimens, **Fig. 8** broken line.

Each data point in the following diagrams corresponds to a single mixed mode experiment (multiple specimen technique). For comparison also the mode I δ_5-Δa curves of centre cracked M(T)- pecimens (2W=250mm and a_0/W=0.3) and C(T) specimens (W=50mm and a_0/W=0.6) are plotted in the diagrams.

Fig. 9 shows the magnitude of the crack tip displacement vector as a function of stable crack growth. All points are positioned between the mode I δ_5-R-curves of the C(T)-. and M(T)-specimens and at least in the initial part of the resistance curves no particular effect of mixed mode loading is discernible. For longer shear crack propagations the R-curve already measured with cruciform specimens under mixed mode loading was obtained. This confirms the finding of (15), where it was stated that the shear crack δ_v-Δa-curve is not influenced by specimen geometry and mixed-mode ratio. The shear crack R-curve did not reach the high δ_5-values of the M(T)-specimens, even if the constraint and therefore the magnitude of the hydrostatic stresses are low under near-mode II loading (6). The cause for this reduction was probably related to the shear crack progressing into prestrained material instead of virgin material between the two shear bands of the symmetric (mode I) case. The stable cracks of the specimens tested at $\phi \leq 60°$ turned after initiation and propagated normally to the loading axis as a mode I crack. The behaviour of the „tensile crack" data points can therefore be explained with the constraint considerations known from mode I (35, 36). Apparently the combination of tensile and bending loading on the kinked crack exerted a constraint of the plastic deformation which laid in between the one of C(T)- and M(T)-specimens (37). Increasing bending components (decreasing ϕ) increase constraint and therefore the δ_v-Δa data points are shifted towards the C(T)-R-curve (ϕ=15° in **Fig. 9**). The δ_5-R-curve of the highly constrained C(T) specimens seems to be a conservative estimation of fracture toughness.

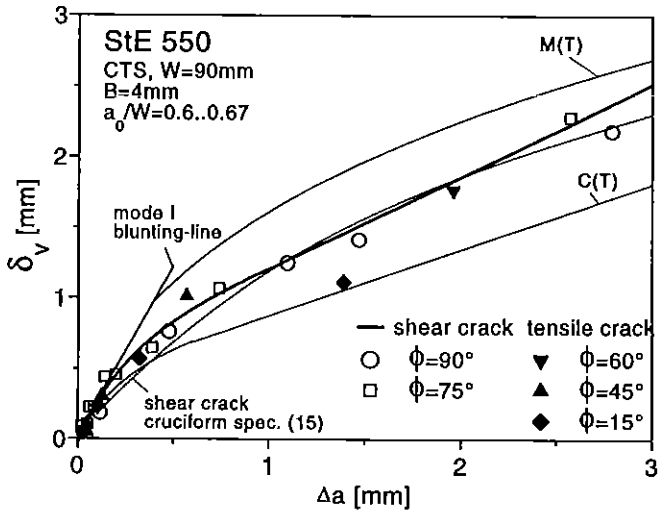

Fig. 9 Optically measured crack tip displacement δ_v versus stable crack growth of the CTS specimens.

Besides for very long propagations of kinked cracks, where all of the investigated J-evaluation methods were invalid, the J-integral crack resistance curves were relatively insensible to the respective J-evaluation method: J_{I+II} in **Fig. 10** and J_{FE} in **Fig. 11**

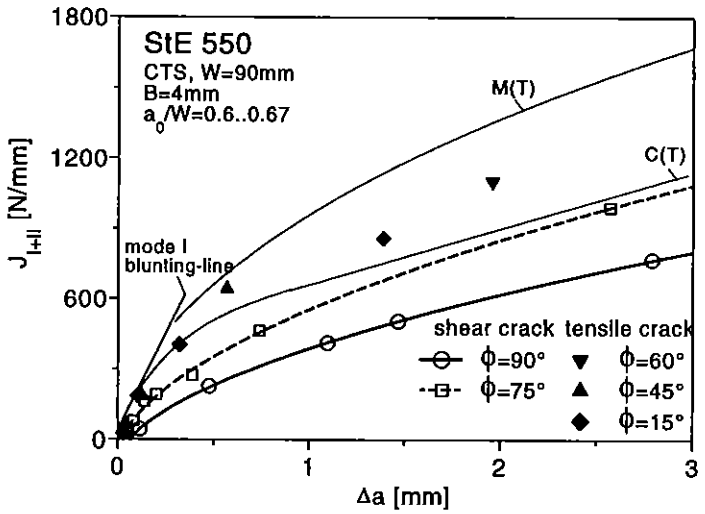

Fig. 10 J integral evaluated with the approach of Thogo and Ishii (eqns. (2) and (8)) versus stable crack growth.

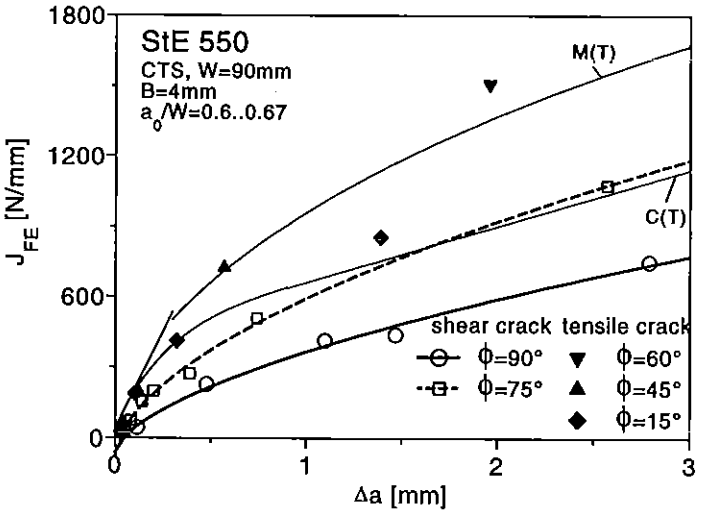

Fig. 11 J integral evaluated with eqns. (2), (3) and the η_{pl}-factor extracted directly from the FE analysis (eqn. (9)) versus stable crack growth

The most obvious feature of the J-Integral crack resistance curves is that the R-curves decrease with increasing mode II loading components. For fixed Δa, the mode II fracture toughness in terms of a J-R-curve was approximately only one half of the mode I J-Δa-curve of a C(T)-specimen. This is an important result, because the various fracture assessment methods relay on J-R-curves of C(T)-specimens, which are believed to be conservative. Also other authors found this decrease of the mode II J-integral tearing resistance in ductile ferritic steels with low work hardening capability or yield plateau (2, 8, 9). These materials fracture under fully plastic conditions and the experimentally obtained J is therefore greatly influenced by the global plastic deformation behaviour of the specimens. In other words: J is, under fully plastic conditions, a somehow calibrated measure of the dissipated plastic energy during (U_{pl}) fracture (38). Knowing that under predominant mode II loading the plastic deformation is localised in the shear band ahead of the crack, whereas extensive plastic zones develop under mode I loading, **Fig. 12**, it is clear that the J tearing resistance must be smaller in mode II than in mode I. In the former case less energy can be dissipated in the narrow shear band.

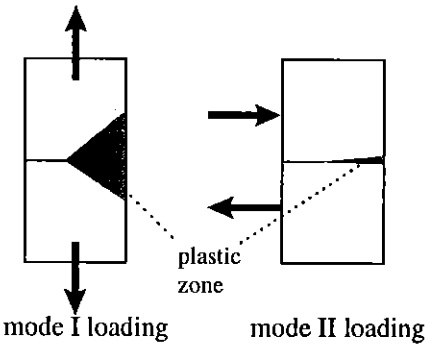

Fig. 12 Plastic flow pattern in mode I and mode II loaded specimens of ductile, low work hardening ferritic steels.

The technical initiation values, taken at Δa=0.2mm and normalised by the geometry independent mode I $\delta_{5,0.2}$- and $J_{I,0.2}$-values are displayed in **Fig. 13**. The differences between a mixed mode fracture characterisation with δ_v and J are evident also in this representation of the results. The crack tip displacement vectors had approximately constant values at incipient crack propagation over almost the entire investigated mixed mode range. On the other hand, $J_{FE,0.2}$ fell off the mode I values as soon as a mode II load component was applied.

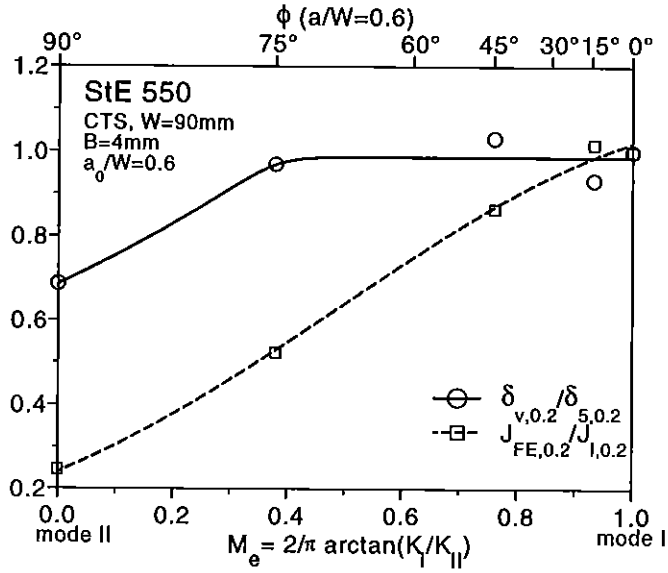

Fig. 13 Technical initiation values (Δa=0.2) normalised by the mode I initiation values as a function of applied mixed mode ratio.

Conclusions

The stable crack propagation direction and crack resistance of thin CTS specimen of a ductile ferritic steel were investigated experimentally. Attention was focused on the suitability of the magnitude of the crack tip displacement vector δ_v and the J-integral to characterise ductile fracture. To obtain the J-values from the load displacement vectors, plastic η-factors had to be developed. For standing cracks, the validity of this J-integral approach was verified with a finite element analysis. The most important results can be summarised as follows:

- Predominant mode I loading components caused a crack path deviation, i.e. the stable crack grew normal to the maximum tensile stress as a mode I crack.
- Under moderate mode II loading, cracks due to shear type fracture grew, with a constant offset of 20°, in the maximum shear strain direction.
- The shear crack resistance curves in terms of δ_v were independent of specimen geometry and mixed mode ratio. They were situated between the resistance curves of mode I C(T)- and M(T)-specimens.

- In case of tensile (mode I) the behaviour of the δ_v-Δa-curves could be explained with the constraint considerations known from mode I ductile fracture.
- The crack tip displacement vectors had approximately constant technical crack initiation values over almost the entire investigated mixed mode range.
- Increasing mode II load components lead to decreasing J-initiation values and lowered the level of the J-R-curves, which fell under the mode I J-Δa-curve of C(T) specimens in case of near mode II loading.
- Because of the unconservatism of the J-R-curves of highly constrained C(T)-specimens and the strong influence of the global specimen deformation behaviour on the mixed mode J-R curves, it can be concluded that the crack tip opening displacement vector δ_v is more appropriate to characterise ductile mixed mode fracture.

References

(1) Maccagno, T.M. and Knott, J.F., (1992), The Mixed Mode I/II Fracture of Lightly Tempered HY130 Steel at Room Temperature, Engng. Fracture Mech., 41, 6, pp. 805-820.

(2) Davenport, J.C.W. and Smith, D.J., (1994), Mixed Mode Ductile Tearing in a Ferritic Steel, Proc. of ECF 10, Vol. 2, (Schwalbe, K.-H. and Berger, C. Eds.), EMAS, pp. 901-910.

(3) Bhattacharjee, D. and Knott, J.F., (1994), Ductile Fracture in HY100 Steel Under Mixed Mode I/Mode II Loading, Acta met., 42, 5, pp. 1747-1754.

(4) Aoki, S., Kishimoto, K., Yoshida, T. and Sakata, M., (1987), A Finite Element Study of the Near Crack Tip Deformation of a Ductile Material Under Mixed Mode Loading, J. Mech. Phys. Solids, 35, 4, pp. 431-455.

(5) Kishimoto, K. and Aoki, S., (1993), Finite Element Analysis on Mixed-Mode Fracture, Mixed-Mode Fatigue and Fracture, ESIS Publ. 14, (Rossmanith, H.P. and Miller, K.J. Eds.), Mech. Engng. Publ., London, pp. 267-284.

(6) Ghosal, A.K. and Narasimhan, R., (1994), A Finite Element Analysis of Mixed-Mode Fracture Initiation by Ductile Failure.Mechanisms, J. Mech. Phys. Solids, 42, 6, pp. 953-978.

(7) Otsuka, A., Thogo, K. and Okamoto, Y., (1987), Relationship Between Ductile Crack Initiation and Void Volume Fraction, Nucl. Engng. Design, 105, pp. 121-129.

(8) Thogo, K., Otsuka, K., and Gao, H.-W., (1990), Behavior of Ductile Crack Initiation from a Crack Under Mixed Mode Loading, J. .Soc. of Mater. Sci. Japan, 39, 443, pp. 1089-1094.

(9) Kardomateas, G. A. and McClintock, F.A., (1987), Test and Interpretation of Mixed Mode I and II Fully Plastic Fracture from Simulated Weld Defects, Int. J. of Fracture, 35, pp. 103-124.

(10) Yoda, M., (1987), The Effect of the Notch Root Radius on the J-Integral Fracture Toughness under Mode I,II and III Loadings, Engng. Fracture Mech., 26, 3, pp. 425-431.

(11) Thogo, K. and Ishii, H., (1992), Elastic-Plastic Fracture Toughness Test Under Mixed Mode I-II Loading, Engng. Fracture Mech., 41, 4, pp. 529-540.

(12) Bank-Sills, L. and Sherman, D., (1991), JII Fracture Testing of a Plastically Deforming Material, Int. J. of Fracture, 50, pp. 15-26.

(13) Richard, H.A., (1981), A New Compact Shear Specimen, Int. J. of Fracture, 17, pp. R105-R107.

(14) Pawliska, P, Richard, H.A. and Buchholz, F.-G., (1992), Bestimmung des Initiierungs- und Ausbreitungsverhaltens von Rissen unter kombinierter ebener Normal- und Schubbeanspruchung mittels Ji-Werte und JR-Kurven, Berichtskolloquium im Schwerpunktprogramm der Deutschen Forschungsgemeinschaft, DVM, Berlin, pp. 83-94.

(15) Dalle Donne, C. and Dõker, H., (1997), Plane Stress Crack Resistance Curves of an Inclined Crack Under Biaxial Loading, Multiaxial Fatigue and Deformation Testing Techniques, ASTM STP 1280, (Kalluri, S. and Bonacuse, P.J. Eds.), ASTM, Philadelphia, pp. 243-263.

(16) Dalle Donne, C., (1997),Übertragbarkeit von Rißwiderstandskurven von Standardproben auf biaxial belastete, bauteilähnlche Kreuzproben, Fortschrittberichte VDI, Reihe 18, Nr. 205, Düsseldorf, VDI Verlag.

(17) Saka, M. and Tanaka, S., (1986), Strain and Stress Fields Near the Blunted Tip of a Crack Under Mixed Mode Loading and the Implications for Fracture, Mech. of Mater., 5, pp. 331-338.

(18) Thogo, K., Otsuka, A. and Gao, H.-W., (1988), Behavior of Ductile Crack Initiation from a Notch Under Mixed Mode Loading, J. .Soc. of Mater. Sci. Japan, 37, 419, pp. 885-890.

(19) Hellmann, D. and Schwalbe, K.-H., (1984), Geometry and Size Effects on J-R and d-R Curves Under Plane Stress Conditions, Fracture Mechanics: Fifteenth Symposium, ASTM STP 833, (Sandford, R.J. Ed.), ASTM, Philadelphia, pp. 577-605.

(20) Amstutz, B.E., Sutton, M.A., Dawicke, D.S. and Newman, J.C., (1995), An Experimental Study of CTOD for Mode I/Mode II Stable Crack Growth in Thin 2024-T3 Aluminum Specimens, Fracture Mechanics: 26th Volume, ASTM STP 1256, (Reuter, W.G, Underwood, J.H and Newman, J.C Eds.), ASTM, Philadelphia, pp. 256-271.

(21) Bradford, R., (1985), Elastic-Plastic Analysis and J-Dominance of the Double Punch Mode II Fracture Toughness Specimen, Int. J. of Fracture, 29, pp. 113-124.

(22) Bank-Sills, L. and Sherman, D., (1990), Elasto-Plastic Analysis of a Mode II Fracture Specimen, Int. J. of Fracture, 46, pp. 105-122.

(23) Jeon, K.L., (1993), Rupture en mode mixte I+II de l' acier inoxidable austénitique 316L, These pour l' obtention du grade de docteur, Ecole Centrale Paris, France.

(24) Sumpter, J.D.G and Turner, C.E, (1976), Method for Laboratory Determination of Jc, Cracks and Fracture, ASTM STP 601, ASTM, Philadelphia, pp. 3-18.

(25) Bucci, R.J., Paris, P.C., Landes, J.D. and Rice, J.R., (1972), J Integral Estimation Procedures, Proc. of the 1971 National Symposium on Fracture Mechanics, ASTM STP 514, ASTM, Philadelphia, pp. 40-69.

(26) Miller, A.G., (1988), Review of Limit Loads of Structures Containing Defects, Int. J. of Pres. Ves. & Piping, 32, pp. 197-327.

(27) Joyce, J.A. and Link, R.E., (1994), Effects of Tensile Loading on Upper Shelf Fracture Toughness, Naval Surface Warfare Center, Carderock Division, CARDIVNSWC-SSM-61-93/23.

(28) Thogo, K., Otsuka, A., Gao, H.-W. and Nojima, Y., (1988), A Simple Method of Estimating the J-Integral for a Mixed-Mode Single Edge Cracked Specimen Subjected to Bending Moment and Shearing Force, Transactions of JSME, Ser. A, A 55, pp. 2307-2315.

(29) Symington, M., Shih, C.F. and Ortiz, M., (1988), Tables of Plane-Strain Mixed-Mode Plastic Crack Tip Fields, Materials Research Group, Division of Engineering, Brown University, Providence, R.I., U.S.A., MRG/DMR-8714665/1.

(30) Chant, M., Green, G., Whatmough, I.J. and Willams, D.C., (1983), The First Large Shear Specimen Test, Central Electricity Generating Board, South Western Region, Bristol, Avon, U.K., SWR/SSD/025/R/83.

(31) Pirondi, A. and Dalle Donne, C., (1996), Crack Propagation in a Ferritic Steel Under Mixed-Mode Loading, XXV AIAS Nat. Conf., Intern. Conf. on Mater. Engn., Vol. II, AIAS, Editrice Salentina Galatina (LE), pp. 969-975.

(32) Ueda, Y., Ikeda, K., Yao, T. and Aoki, M., (1983), Characteristics of Brittle Fracture Under General Combined Modes Including Those Under Bi-Axial Tensile Loads, Engng. Fracture Mech., 18, 6, pp. 1131-1158.

(33) Beachem, C.D., (1975), The Effects of Crack Tip Plastic Flow Directions Upon Microscopic Dimple Shapes, Met. Trans. A, 6A, pp. 377-383.

(34) Kardomateas, G.A., McClintock, F.A. and Carter, W.T., (1985), Directional Effects in Asymmetric Fully Plastic Crack Growth, Engng. Fracture Mech., 21, 2, pp. 341-351.

(35) Kirk, M.T. and Bakker, A., Editors, (1995),Constraint Effects in Fracture Theory and Applications: Second Volume, ASTM STP 1244, Philadelphia, ASTM.

(36) Hackett, E.M., Schwalbe, K.-H. and Dodds, R.H, Editors, (1993),Constraint Effects in Fracture, ASTM STP 1171, Philadelphia, ASTM.

(37) Hallbäck, N. and Jönsson, N., (1996), T-Stress Evaluations of Mixed-Mode I/II Fracture Specimens and T-Effects on Mixed-Mode Failure of Aluminium, Int. J. of Fracture, 76, pp. 141-168.

(38) Kolednik, O., (1991), On the Physical Meaning of the J-Da-Curves, Engng. Fracture Mech., 38, 6, pp. 403-412.